SAND2023-05232C

Performance Evaluation of a Dual Wound Generator for Naval Power System Applications

Timothy Donnelly
Electrical Sciences and Experiments
Sandia National Laboratories
Albuquerque, New Mexico 87125
Email: tjdonne@sandia.gov

Lee Rashkin
Electrical Sciences and Experiments
Sandia National Laboratories
Albuquerque, New Mexico 87125
Email: lrashki@sandia.gov

Marvin Cook
Systems Research Department
Sandia National Laboratories
Albuquerque, New Mexico 87125
Email: macook@sandia.gov

***Abstract*—The ongoing electrification of land, air, space, and sea vehicle systems has placed an increased level of importance on the design and architecture choices of their respective electric power delivery networks. In this work, the performance of a multi-bus medium voltage dc system that is representative of future Navy Electric Warship ambitions is evaluated. The selected system topology is based around a dual wound generator with actively controlled rectifiers. Experimental results demonstrate that such a system can supply multiple buses from the same source while maintaining strong isolation between them. These results – along with a demonstration of system-level performance including the integration of dual-fed loads and energy storage – provide a useful reference for designers tasked with developing reliable and cost-effective power system solutions in these new and emerging environments.**

I. Introduction

The next generation of power systems being developed for land, air, space, and sea vehicles has the potential to provide unsurpassed performance, efficiency, size, weight, reliability, and cost savings over conventional approaches [1] [2]. This is due to the electrification of these systems with designs based on modern power electronics. The flexibility afforded by power electronics to quickly and accurately control power flows has opened the door to a variety of novel power system designs and formulations. Among these, multi-bus medium voltage dc (MVDC) systems have received significant interest, particularly by the Navy for future electric warships [3].

Multi-bus designs can offer increased reliability compared to single bus systems, however a size/weight/cost penalty can also arise if each bus has its own independent energy generation. This has led to the consideration of single-source, multi-bus architectures which can offer an effective trade-off between these competing objectives [4]. Previous research in this vein has shown that a dual-wound generator (DWG), a machine with two different windings sharing the same stator, makes an ideal source candidate for such a topology [5] [6] [7]. This is because the outputs of the generator can be rectified to create two dc buses with relatively favorable bus-to-bus isolation. Nevertheless, because the two windings of the DWG are part of the same electromechanical system, some degree of coupling between the buses remains.

This work extends the research of [5] [6] [7] and considers the performance of a DWG-based power system that utilizes controllable rectifiers on the generator outputs, and investigates the impact on coupling associated with the addition of other power system components such as dual-fed loads (DFL) and energy storage systems (ESS). The remainder of the paper is organized as follows: in Section II, the details of the power system and associated equipment is provided; in Section III, experimental results comparing the performance of a passively rectified system to actively rectified system are conveyed; in Section IV, the impact of droop controls, the addition of a DFL, and the addition of ESS into the system are considered. Finally, in Section V, a conclusion is provided and directions for future research are identified.

II. System Description

A schematic of the single source, multi-bus power system considered in this work is shown in Fig. 1. The system is based around a dual wound generator which is a permanent magnet synchronous machine (PMSM) that has two galvanically isolation three-phase windings, which are offset by 60° [5]. The system is representative of a potential single zone configuration in a future Navy Electric Warship: including generation, service loads, energy storage, and a representative high reliability and/or high power dual-fed load. Examples of such a dual-fed load in naval applications include propulsion motors, directed energy weapons, and electromagnetic aircraft launch systems (EMALS) [8].

The system shown in Fig. 1 was implemented in hardware on the Secure Scalable Microgrid Test Bed (SSMTB) at Sandia National Laboratories [9]. The SSMTB has the ability to emulate multiple dc microgrids, including a variety of loads, sources, converters and a communications and control network overlay to coordinate power management among them. A illustration of the overall SSMTB and a few examples of associated equipment are shown in Fig. 2. Part of the SSMTB design includes emulators for various sources, and the DWG in this case was driven mechanically by an induction motor that emulates the dynamic behavior of a diesel engine [10]. An image of the diesel emulator and DWG hardware is shown in Fig. 3.

On the ac side of the DWG, a pair of active rectifiers are used to create two independent dc buses. Control of the active rectifiers is primarily accomplished through a real-time

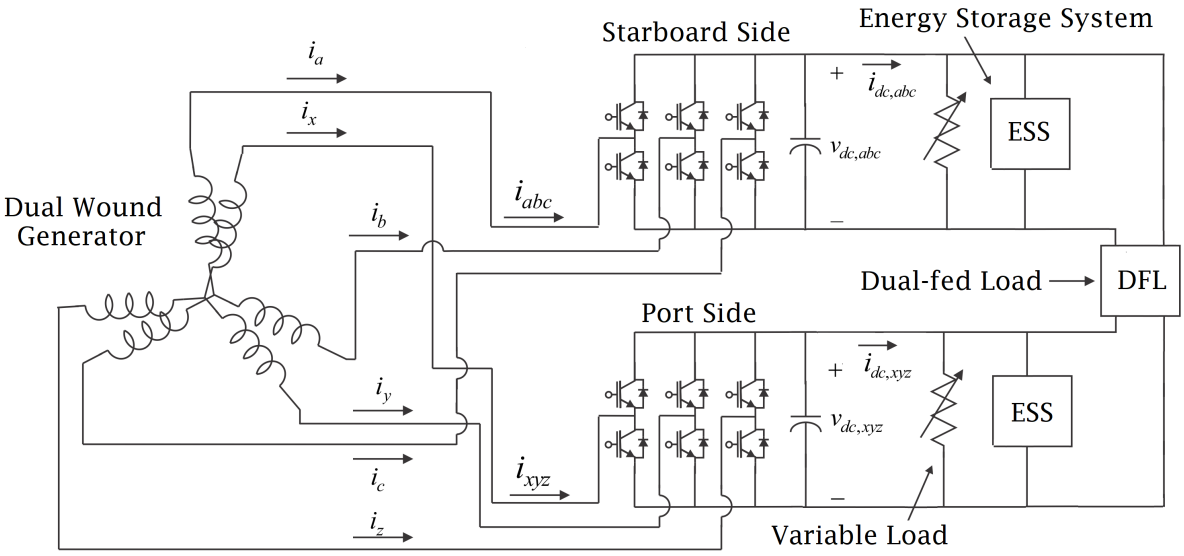

Fig. 1. Schematic illustration of the dual wound generator-based two-bus dc power system

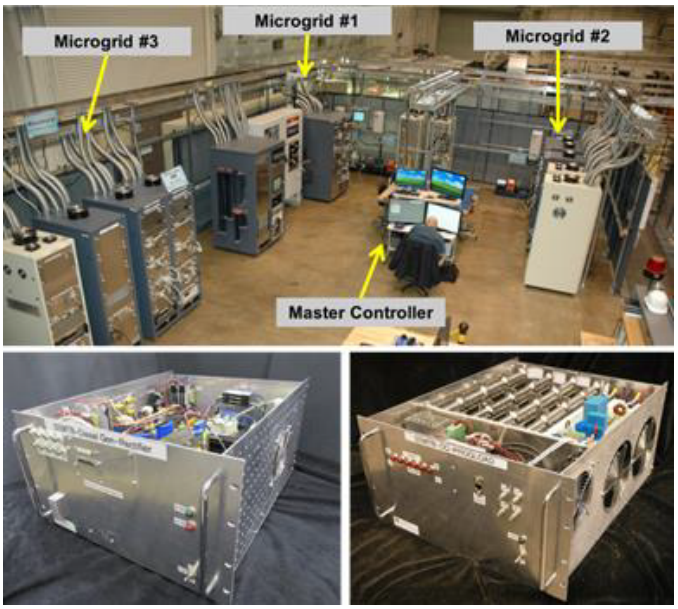

Fig. 2. Photos of (top) the microgrid testbed, (bottom left) rectifier, and (bottom right) 6.7kW digital resistor

Fig. 3. Diesel generator emulator and dual-wound generator (bottom), drive and controller for diesel emulator shown above

Speedgoat controller [11]. The controller measures the angular position of the rotor, the output dc voltages/currents, and the ac currents for each winding. Feedback controls are then used to calculate the desired space vector modulation (SVM) switching signals for each rectifier. A control block diagram for the DWG system is shown Fig. 4. The voltage controller is based on [6], and includes a provision for droop output regulation. The active rectifier hardware is based on a *CREE* SiC power MOSFET module [12], and switches at a frequency of 40kHz.

In addition to the active rectifier controls, a separate LabView application running on a desktop computer is also used to control the load profiles of the power system. An example load profile is shown in Fig. 5. This profile varies the resistive load on the starboard (abc) side in the shape of a chirp signal, and leaves the port (xyz) side at fixed value. This profile is used to evaluate the isolation that can be achieved between the two buses of the power system by injecting a broad-band disturbance on one bus, and measuring the corresponding variation in voltage on the other bus. The dynamic regulation performance of a single bus can also be evaluated by measuring the voltage variation on the same bus as the chirp disturbance.

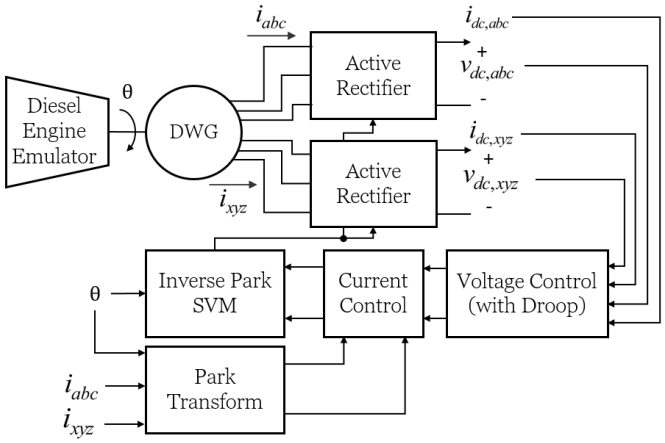

Fig. 4. Control block diagram for output voltage regulation of active rectifier

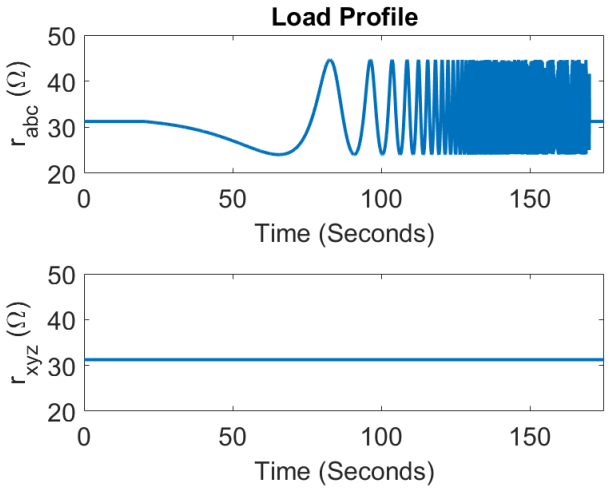

Fig. 5. Chirp load profile for characterizing dual wound generator electromagnetic coupling characteristics

III. Bus-to-Bus Isolation: Passive vs Active Rectification

One key metric to evaluate the performance of a single-source, multi-bus power system is the measure of isolation that exists between the independent buses. This metric is important since a decoupled system would indicate that disturbance on one bus, such as fault, will not propagate to the other buses – thus providing the reliability expected of a multi-bus system. In this section, the impact that passive vs. active rectification can have on system isolation is provided, along with a description of how the coupling can be quantified.

For this test, the diesel engine emulator driving the dual-wound generator was configured to regulate a constant speed of 680rpm. The load profile for the starboard (abc) and port (xyz) sides was configured as shown in Fig. 5, and the ESS and DFL were disconnected from the system. Fig. 6 shows the dc output voltages for both the starboard- and port-sides during this test. Two separate studies were performed: (left) when SVM switching was disabled and the rectifiers operate passively, and (right) when SVM switching was enabled.

From Fig. 6, it is visually clear that for the passive rectifiers, a varying load on the starboard side strongly influences the output voltage on the port side. In contrast, less coupling between the starboard and port sides is seen for the active rectifiers, although there is more high frequency switching noise. This is due to the fact that the active rectifiers use feedback controls to regulate each bus independently, whereas the passive rectifier coupling is driven purely by physical dynamics [6]. It is also noted that the passive rectifiers generate an output voltage of approximately 107Vdc, which is below the nominal 200Vdc for this system. Although higher voltages could be obtained with increased speed, the coupling dynamics can be better understood by keeping speed fixed and instead computing a transfer function which scales the measured voltage disturbance on each bus by the respective power disturbance, as discussed next.

In the frequency domain, the coupling between the voltage of a bus and the load on that same bus or an adjacent bus can be quantified by computing a corresponding transfer function (TF) [7], as in:

$$H_{self} = \frac{\tilde{V}_{dc,abc}}{\tilde{P}_{abc}}, \quad H_{cross} = \frac{\tilde{V}_{dc,xyz}}{\tilde{P}_{abc}} \tag{1}$$

where $v_{dc,abc}$ and $v_{dc,xyz}$ correspond to the starboard and port bus voltages, p_{abc} corresponds to the power being dissipated by the chirp load profile, and tilde is used to indicate frequency domain-signals, i.e., $\tilde{X} = \texttt{fft}(x)$. The power being dissipated by the chirp load was measured by taking the product of the measured voltage across the resistor bank and the measured current entering the resistor bank. A comparison between the self and cross coupling (starboard-to-starboard, vs. starboard-to-port) for the passively and actively rectified systems is shown in Figs. 7(a) and 7(b), respectfully.

From Fig. 7, it is clear that the actively rectified DWG is less coupled than the passively rectified system, on the order of 20dB or more in the low frequency range, which is in agreement with expected results from Fig. 6. It is noted that at higher frequencies, however, the difference in coupling between the passive and active rectifiers is diminished. This is due to the control bandwidth of the active rectifiers, which is estimated to be approximately 0.5 Hz. Above this frequency, the active rectifiers are unable to regulate output voltage, leading to the similar behavior between the passive and active systems.

IV. System-level Performance

In a system-setting, the individual design of each component, and the interaction between multiple components, can have an major impact on the bus-to-bus isolation. This section investigates some of these considerations by introducing components shown in Fig. 1 one at a time, and in the end providing coupling transfer function results for a complete system.

A. Impact of Droop

In a system with multiple sources that can supply energy to the same bus, a droop control scheme is often used to

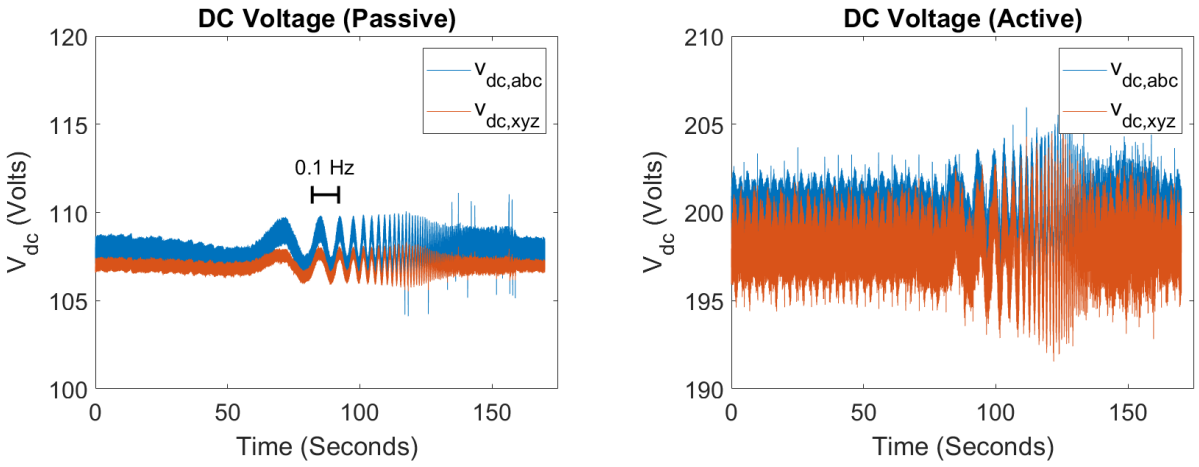

(a) (b)

Fig. 6. Recitifer dc output voltages for the chirp load profile: (a) passive recitifcation, (b) active recitification

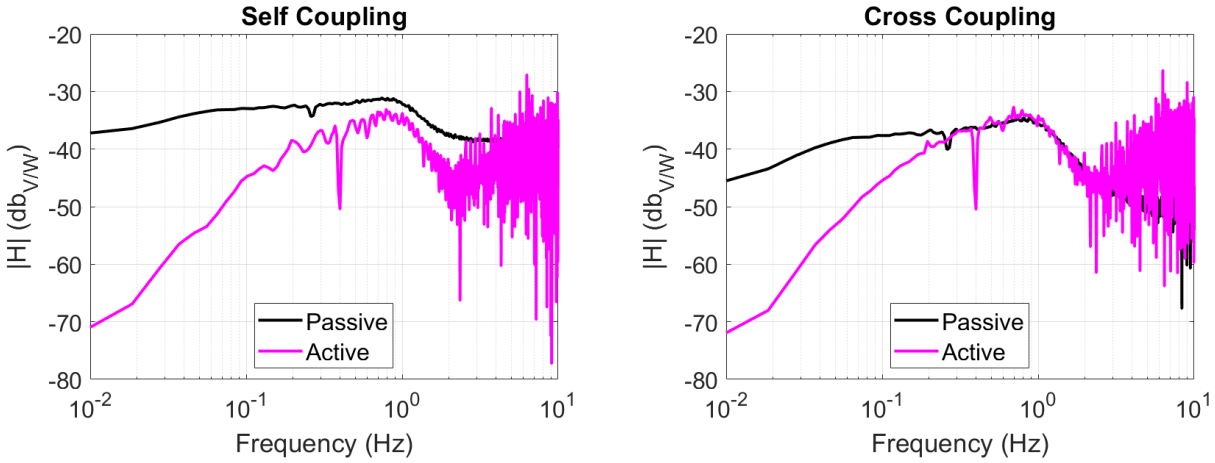

(a) (b)

Fig. 7. Self and cross coupling transfer functions for DWG with both passive and active rectification

coordinate power flow. In this work a droop control of the form:

$$e = (V_{dc}^* - V_{dc}) - K_d(I_{dc}^* - I_{dc}) \tag{2}$$

was used where V_{dc}^* and I_{dc}^* are the commanded dc voltage and current values, V_{dc} and I_{dc} are the corresponding measured values, and e is the voltage error term fed into voltage regulator, which is driven to zero in steady-state. The introduction of a commanded current value in (2) allows the power sharing between DWG and other components, such as the ESS, to be controlled more accurately and will be discussed later.

In order to study the effect that droop control can have on the coupling of the DWG, a chirp test was conducted with initially only the DWG and programmable loads connected in the system. The droop parameter was varied from $K_d = 1, 5, 10\Omega$, and the corresponding self and cross coupling transfer functions are shown in Fig. 8. At dc and for low-frequencies that are within the control bandwidth of the active rectifier, the output impedance of the DWG for both the starboard and port-sides is expected to be the corresponding droop resistance. Thus as the droop parameter increases, the self coupling TF is also expected to increase, since the current being delivered to a time-varying load must flow through a larger resistance. For similar reasons, the cross-coupling TF also increases at low-frequencies as the droop parameter is increased. For higher frequencies, however, the droop parameters plays a less significant role and instead the cross-coupling between busses is dominated by the mutual inductance of the windings.

It is noted that droop parameter not only effects the dc-side dynamics of the DWG, but influences the ac-side and mechanical dynamics as well. When a smaller droop coefficient is used, the active rectifiers are more responsive to changes in load. Since the power leaving the active rectifier must ultimately come from the mechanical source, this corresponds to larger torque demands being placed on the diesel engine and thus

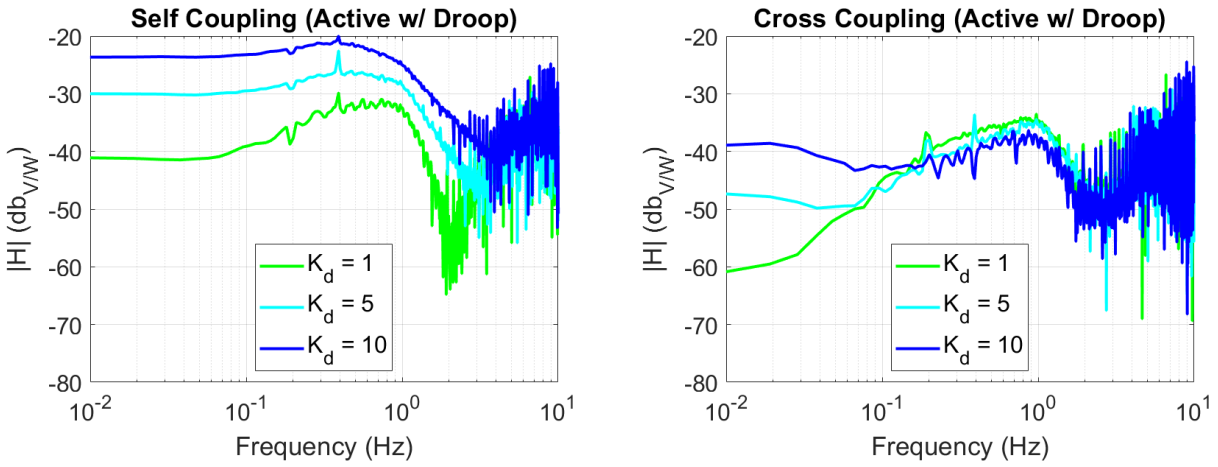

(a) (b)

Fig. 8. Self and cross coupling TFs for a DWG with active rectifiers and various droop parameter settings

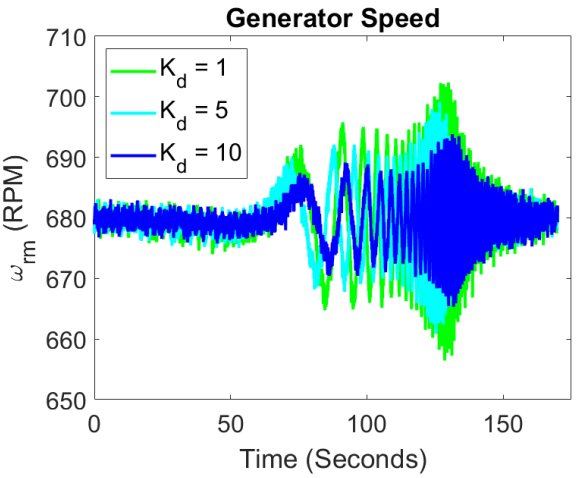

Fig. 9. Generator speed for various droop parameter settings

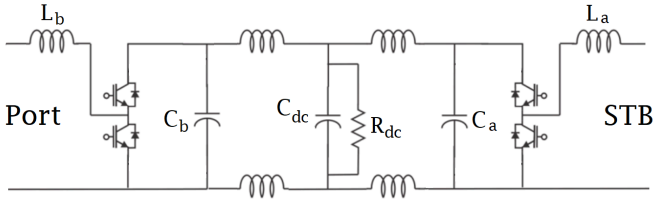

Fig. 10. Schematic illustration of the dual-fed Load (DFL), which is connected between the Starboard (STB) and Port buses

more engine speed variation. A plot of the generator speed for the various K_d parameters is shown in Fig. 9. As expected, the smaller the value of K_d, the larger variation in speed. Although a detailed analysis of how this speed variation could impact mechanical systems is outside the scope of this work, a further demonstration of how the speed variation is impacted by the addition of energy storage into the system is provided in Section IV-C.

B. Impact of Dual-fed Load

Along with the impact that the droop parameter can have on the self- and cross-coupling TFs, the inclusion of additional circuit components can also have an impact. Here the DWG with active rectifiers was used to supply a dual-fed load (DFL). A schematic of the DFL is shown in Fig. 10, which consists of two boost-converters, each feeding a central capacitor/load combination. The DFL is configured to regulate the central dc capacitor voltage to a fixed value (300 Vdc), and equal current draws are commanded from each side to achieve this goal. Thus in steady-state the current entering the DFL from each side is expected to be the same, however during transients these currents may differ.

With the DFL as part of the circuit, another chirp test was conducted and the self- and cross-coupling TFs are shown in Fig. 11. The self-coupling TF strongly resembles the TF shown in Fig. 8(a) – implying the dynamics of the self-coupling mechanism are dominated by the dynamics of the active rectifier, and the dual fed load has little effect. In contrast, the cross-coupling TF changes considerably from Fig. 8(b) to Fig. 11(b) with the introduction of the DFL. Interestingly, the coupling between the two busses decreases (at least in the low-frequency regime) with the introduction of a component sitting between the two busses. This occurs because the power being delivered to the DFL from each bus is adjusting in real time to the respective loads on each bus, thus allowing for the chirp load on one side to be sourced indirectly by both buses, decreasing the voltage variation on either side.

C. Impact of Energy Storage

Energy storage systems have been proposed as a effective solution for mitigating the impact of transient disturbances in electrical power systems, particularly in microgrid and mobile power system applications with limited spinning reserve [3]. The impact of introducing ESS to the DWG-based power

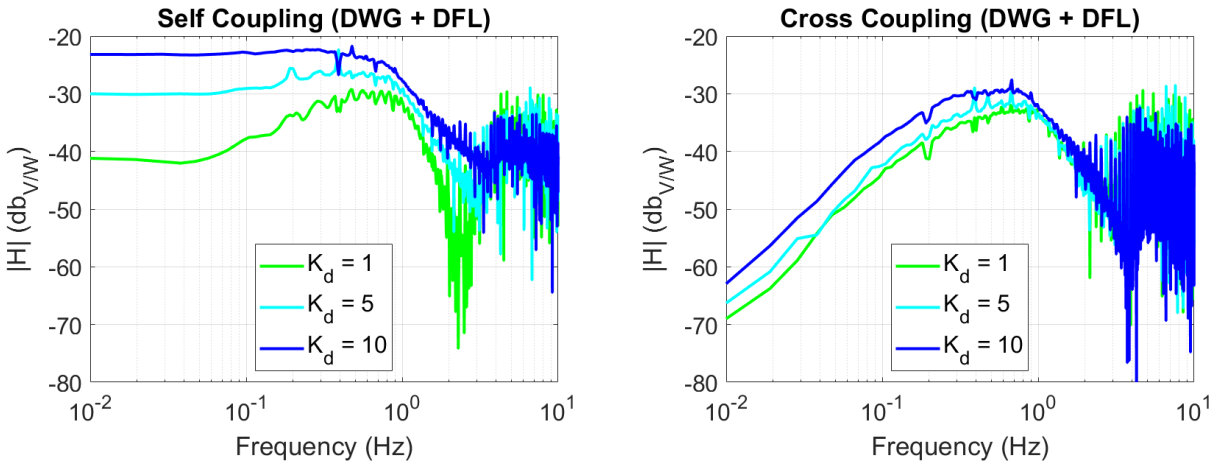

(a) (b)

Fig. 11. Self and cross coupling TFs for a DWG + DFL power system.

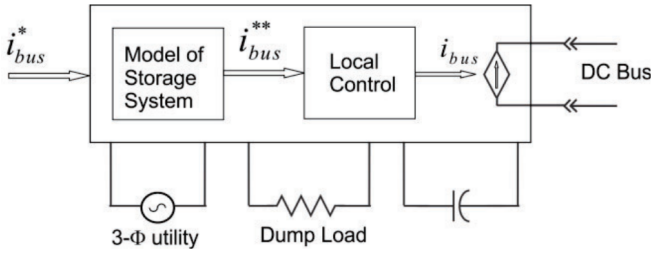

Fig. 12. Energy storage system (ESS)

system is evaluated in this section. A high-level schematic representation of the ESS is shown in Fig. 12; the ESS is configured so that is can both source and sink power. For this test, the controls of the ESS are configured to regulate a constant dc output voltage with a $K_d = 1\Omega$ droop term included.

A final chirp test was conducted with the DWG, DFL, and one ESS on each bus. The corresponding self- and cross-coupling TFs are shown in Fig. 13. Compared to Fig. 11(a) which did not include the ESS, the self-coupling of the system with energy storage is much reduced. This is expected, since the ESS will work to regulate the voltage of the dc bus and either source or sink power in response to a disturbance such as a chirp load profile being applied.

As was the case for the self-coupling TF, the cross-coupling TF shown in Fig. 13(b) is also much reduced compared to Fig. 11(b) with the introduction of the ESS. This is again because the ESS is able to supply and sink power on both of the power system busses, thus ensuring that a disturbance on on-side has minimal impact on the other bus. It is noted that a resonance at approximately 2 Hz is observed in both the self- and cross coupling TFs shown in Fig. 13, which becomes more apparent as the droop parameter is decreased. This resonance is due to the interaction between the DWG and the ESS, and its impact on generator speed is discussed next.

As discussed in Section IV-A, the dynamics on the dc side of the DWG also impacts the mechanical side. A plot of the generator speed when energy storage is present in the system is shown in Fig. 14. Compared to Fig. 9, there is much less speed variation as the energy storage is able to help compensate for the changing chirp load profile. It is noted that at approximately $t = 130$, a large variation in speed is observed for the case $K_d = 1$. This point in time corresponds to the point in the chirp signal when the load is varying at approximately 2 Hz, which is at the resonance of the system.

The full impact that this resonance may have on system performance is still under investigation, however it is noted that by using a large droop coefficient such a $K_d = 10$, the generator acts more like a constant power source instead of a voltage source. Although this could lead to large voltage variations if the system does not contain energy storage (Fig. 8), with energy storage one can obtain the best of both worlds: small speed variation on the generator, with low self- and cross- coupling between buses.

V. Conclusion

A single source, multi-bus power system based around a dual-wound generator is presented in this work. Experimental results demonstrate there are several factors that can influence the degree of bus-to-bus isolation that can be achieved with this topology. It was demonstrated that the impact of; passive vs active rectification, droop control, adding other system components that span multiple busses, and energy storage systems, can help to reduce self- and cross-coupling effects in such a system. Directions of future research are anticipated to focus on additional control schemes besides droop control that can maintain strong bus isolation, and further investigation into how other common power-system components can impact system performance.

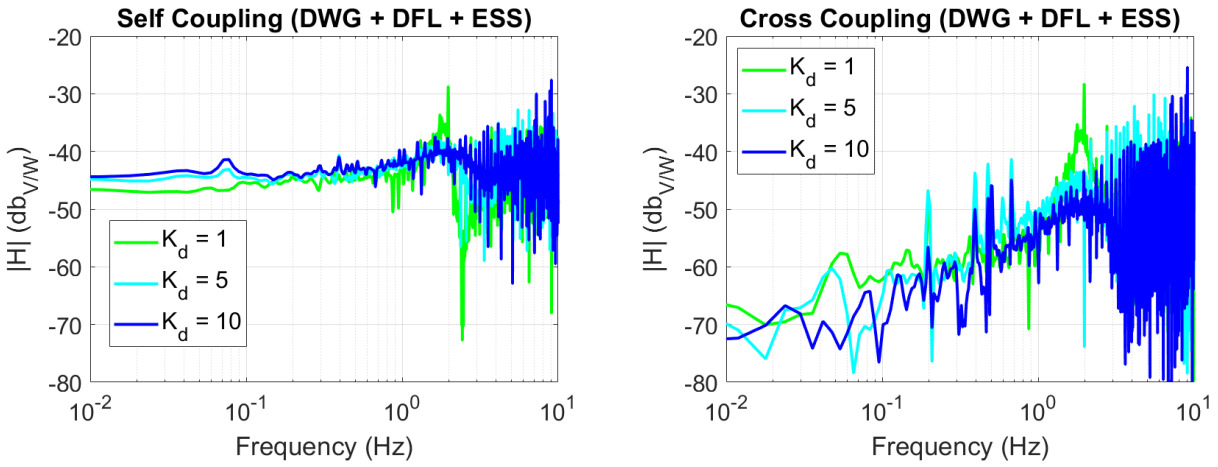

(a) (b)

Fig. 13. Self and cross coupling TFs for a DWG with active rectifiers feeding a chirp load on one bus, a DFL on both buses, and both buses being supported by voltage controlled ESS

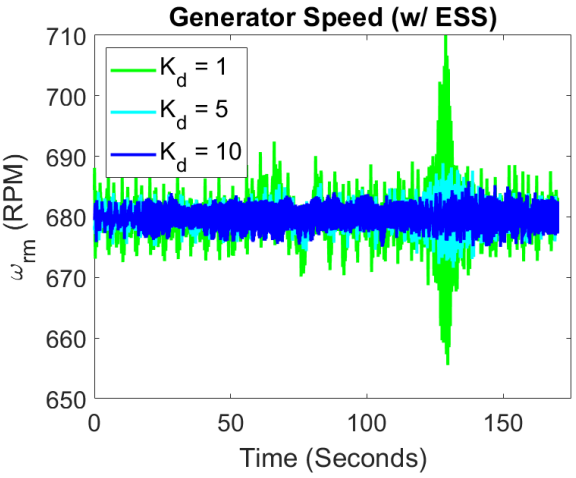

Fig. 14. Generator speed for various droop parameters in a system with energy storage

ACKNOWLEDGMENT

This work was supported by the Office of Naval Research and the Electric Ships Office for a project entitled Nonlinear Power Flow Control Design for NGIP Energy Storage Requirements, PR# 1400354102. In addition, the authors would like to thank David Wilson for his technical review of this work. This article has been authored by an employee of National Technology & Engineering Solutions of Sandia, LLC under Contract No. DE-NA0003525 with the U.S. Department of Energy (DOE). The employee owns all right, title and interest in and to the article and is solely responsible for its contents. The United States Government retains and the publisher, by accepting the article for publication, acknowledges that the United States Government retains a non-exclusive, paid-up, irrevocable, world-wide license to publish or reproduce the published form of this article or allow others to do so, for United States Government purposes. The DOE will provide public access to these results of federally sponsored research in accordance with the DOE Public Access Plan.

REFERENCES

[1] A. Emadi, "Transportation 2.0," *IEEE Power and Energy Magazine*, vol. 9, no. 4, pp. 18–29, Jul.-Aug. 2011.

[2] M. A. Tamor and E. B. Stechel, "Electrification of transportation means a lot more than a lot more electric vehicles," *iScience*, vol. 25, no. 6, Jun 2022.

[3] N. Doerry and J. Amy Jr., "The road to MVDC," in *ASNE Intelligent Ships Symposium 2015*, Philadelphia, PA, May 20-21, 2015.

[4] C. G. Hodge and J. F. Eastham, "Dual wound machines for electric ship power systems," in *2015 IEEE Electric Ship Technologies Symposium (ESTS)*, 2015, pp. 62–67.

[5] L. J. Rashkin, J. C. Neely, S. F. Glover, T. J. McCoy, and S. D. Pekarek, "Dynamic considerations of power system coupling through dual-wound generators," in *2017 IEEE Electric Ship Technologies Symposium (ESTS)*, 2017, pp. 493–500.

[6] L. J. Rashkin, J. C. Neely, S. F. Glover, T. J. McCoy, and N. Doerry, "Dynamic response evaluation of a 20 mw scale dual wound machine based power system," in *Advanced Machinery Technology Symposium 2018*, Philadelphia, PA, March 20-21, 2018.

[7] L. Rashkin, R. Matthews, J. Neely, and N. Doerry, "Dynamic response comparison of dual-wound and single-wound machines in multi-bus power system architectures," in *2020 IEEE Transportation Electrification Conference & Expo (ITEC)*, 2020, pp. 784–788.

[8] J. Neely, L. Rashkin, M. Cook, D. Wilson, and S. Glover, "Evaluation of power flow control for an all-electric warship power system with pulsed load applications," in *2016 IEEE Applied Power Electronics Conference and Exposition (APEC)*, 2016, pp. 3537–3544.

[9] S. Glover, J. Neely, A. Lentine, J. Finn, F. White, P. Foster, O. Wasynczuk, S. Pekarek, and B. Loop, "Secure scalable microgrid test bed at sandia national laboratories," in *2012 IEEE International Conference on Cyber Technology in Automation, Control, and Intelligent Systems (CYBER)*, 2012, pp. 23–27.

[10] J. C. Neely, S. Pekarek, S. Glover, J. Finn, O. Wasynczuk, and B. Loop, "An economical diesel engine emulator for micro-grid research," in *International Symposium on Power Electronics Power Electronics, Electrical Drives, Automation and Motion*, 2012, pp. 175–179.

[11] *Performance Real-Time Target Machine*, Speedgoat GmbH, 2023. [Online]. Available: https://www.speedgoat.com/

[12] *Hex SiC N-Channel MOSFET 29 A CCS020M12CM*, Wolfspeed. [Online]. Available: https://www.wolfspeed.com/